


Mesoporous SBA-15 Silica-Loaded Nanoformulation of Quercetin: A Probable Radio-Sensitizer for Lung Carcinoma

Dose-Response:
An International Journal
January-March 2022:1–10
© The Author(s) 2022
Article reuse guidelines:
sagepub.com/journals-permissions
DOI: 10.1177/15593258211050532
journals.sagepub.com/home/dos


Saad Alkahtani¹ , Saud Alarifi¹ , Nada H. Aljarba², Hamzah A. Alghamdi¹, and Abdullah A. Alkahtane¹

Abstract

Lung cancer is considered as one of the most serious disease worldwide. The progress of drug carriers based on nonmaterial, which selectively hold chemotherapeutic agents to cancer cells, has become a major focus in biomedical research. This study aimed to evaluate the growth inhibition and apoptosis induction of the human lung cancer cells (A-549) by Q-loaded SBA-15 conjugate system. Mesoporous silica nanoparticles (SBA-15) as host materials for transporting therapeutics medicaments were fabricated for targeted drug delivery toward lung cancer. With the objective of increasing bioavailability and aqueous solubility of flavonoids, SBA-15 was successfully loaded with the quercetin (Q)—a major flavonoid and characterized with the help of Fourier-transform infrared spectroscopy (FTIR) and transmission electron microscopy (TEM). The biological investigation on A549 cell line confirmed that the efficacy of Q-SBA-15 is much higher than only Q. Moreover, the apoptotic pathway of synthesized Q-SBA-15 NPs examined that the Q-SBA-15-mediated apoptosis *via* PI3K/AKT/mTOR signaling pathway. Thus, the newly conjugated Q-SBA-15 system improved the apoptotic fate through caspase-mediated apoptosis *via* PI3K/AKT/mTOR signaling pathway and hence, it can be potentially employed as an anticancer agent for lung cancer.

Keywords

lung cancer, quercetin, nanoparticles, apoptosis, mesoporous

Introduction

Lung cancer has emerged as major cause of oncological death worldwide, with neoplasia being generally avoidable by weight control, intake of vegetable food, and reduction of alcohol and tobacco. Owing to the complex molecular biology associated with lung metastases, various therapeutics approaches have been assumed such as chemotherapy, radiotherapy, and immunotherapy capable of defeating tumor growth to some extent.¹⁻⁴ Among them, majority of lung cancer treatment requires ionizing radiation (IR) to destroy proliferating cells and exhibits a crucial role in native control after surgery.^{5,6} In the course of radiotherapy, ionizing radiation damages the cancerous DNA, thereby facilitating tumor cell apoptosis and necrosis in cancerous tissues.^{7,8} Regardless of current improvements in radiation therapy (RT), there are still certain limitations to its use *viz.*: (a) failed to differentiate healthy and infectious tissue, (b) radiation dosage and hence

its therapeutic effects, and (c) intrinsic radiation resistance arises due to incomplete tumor response or recurrence.⁹⁻¹¹ Therefore, a new strategy is required to lower these issue laid by association between IR and photosensitizers that potentiate the radiotherapy outcomes.¹²⁻¹⁴ One probable area of development is the use of biomaterial-based radioprotective agent to combine the effects of RT with other therapeutic modalities.^{3,13,15,16} Literature reports presented that the

¹Department of Zoology, College of Science, King Saud University, Riyadh, Saudi Arabia

²Department of Biology, College of Sciences, Princess Nourah Bint Abdulrahman University, Riyadh, Saudi Arabia

Corresponding Author:

Saad Alkahtani, Department of Zoology, College of Science, King Saud University, P. O. Box 2455, Riyadh 11451, Saudi Arabia.
Email: salkahtani@ksu.edu.sa



Creative Commons Non Commercial CC BY-NC: This article is distributed under the terms of the Creative Commons Attribution-NonCommercial 4.0 License (<https://creativecommons.org/licenses/by-nc/4.0/>) which permits non-commercial use, reproduction and distribution of the work without further permission provided the original work is attributed as specified on the SAGE

and Open Access pages (<https://us.sagepub.com/en-us/nam/open-access-at-sage>).

antioxidants derived either from exogenous/endogenous sources provide defense system to the body and neutralize excess reactive oxygen species (ROS) to diminish the injury governed by IR-induced.^{17,18}

In this context, natural occurring bioflavonoids have great therapeutic potential against various cancers as they are involved in a different signaling pathway related to apoptosis *via* modulating gene expression.¹⁹ In particular, Q (3,3,4,5,7-pentahydroxyflavone) is of the special interest for its diverse biological effects, inhibiting multiple enzymes involved in cell proliferation, including antiproliferative and apoptotic pathways.²⁰⁻²² It can also act as chemoprotective and radio-protective agent, protecting normal cells from the side effects, which offers notable benefits in anticancer treatment.^{16,23} Moreover, it induces mitochondrial mediated both up- and down-regulation of pro-apoptotic proteins with the release of *cytochrome c*.²¹⁻²⁵ As an effective ROS scavenger, Q exerts an antioxidant property which helps in the free radical-scavenging, reducing the level of ROS and inhibiting lipid peroxidation.^{26,27} However, its clinical efficacy is restricted mainly due to low polar solubility and chemical instability that eventually lead to insufficient accumulation around cancer cell.^{23,28} Thus, alternative schemes based on multifunctional nanomaterials have been carried out to improve the aqueous solubility of Q and radiation responses and thereby achieving enhanced RT with reduced radio-toxicity.^{29,30}

Mesoporous silica nanoparticulate (MCM-41, MCM-48, and SBA-15) has been familiarized for the drug delivery purposes and still they are being investigated.^{31,32} SBA-15 is

one of the common 2D hexagonally arrayed mesoporous materials which ensures the easy access of drug molecules due to its biocompatibility and a low cytotoxicity.^{32,33} The kinetic release of the drug molecule can be control by the modulating the pore diameter pore diameter, which directs the expulsion of from SBA-15.³⁴ It is imperative to analyze the biological effects of Q-loaded SBA-15 mesoporous nanomaterial induce cytotoxicity.

Although several studies regarding the encapsulation of quercetin by other nanoparticulate system have been documented in literature, however cytotoxicity studies of SBA-15 encapsulated Q against lung cancer are scarcely reported. Present investigation aimed to evaluate the growth inhibition and apoptosis induction of the human lung cancer cells (A-549) by Q-loaded SBA-15 conjugate system (Figure 1). Furthermore, we determined that the efficacy of Q-SBA-15 is better than only Q alone. Therefore, we conclude that the coupling of antioxidant to mesoporous silica nanoparticles as a new carrier that generates lower oxidative stress and beneficial in term of ROS reduction, cellular viability, and protective effects mediated apoptosis pathway involved *via* AKT/PI3K/mTOR axis.

Experimental Section

Chemical and Cell Lines

P123 (Poly (ethylene glycol)-block-poly (propylene glycol)-block-poly (ethylene glycol), TEOS (tetraethyl orthosilicate) were procured from Sigma Aldrich, United States.

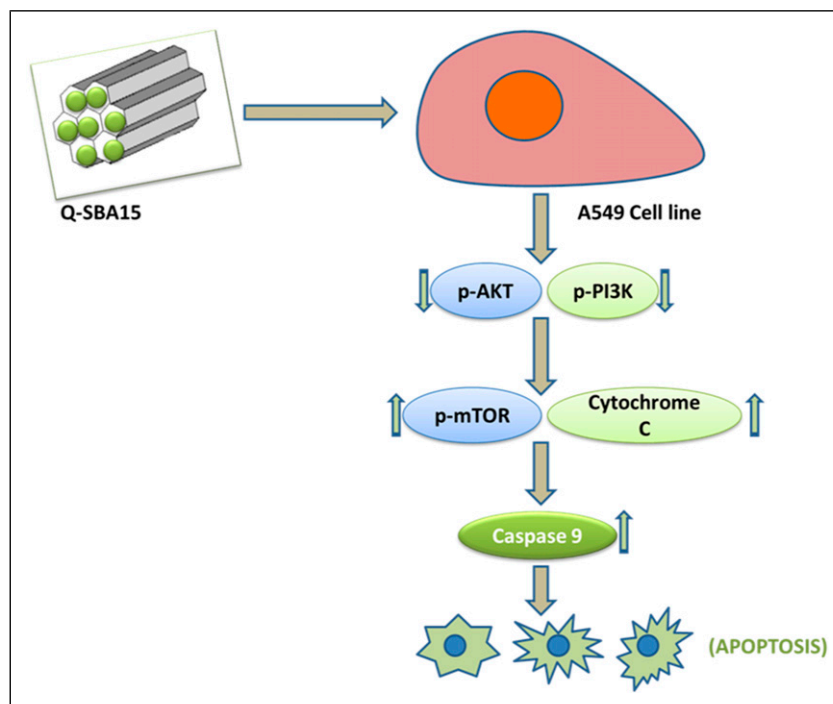


Figure 1. Diagram showing Q-loaded SBA-15 conjugate system and its mode of action.

Human lung carcinoma (A549) cell line of passage four was acquired from ATCC, United States. Cell culture media components: trypsin, DMEM, FBS, PSN antibiotic cocktail, and EDTA were purchased from Gibco (Grand Island, NY, United States). Antibodies were procured from Santa Cruz Biotechnology, Dallas, Texas, United States and eBioscience, San Diego, United States. Dyes were bought from Thermo Fisher Scientific, United States.

Synthesis of Mesoporous SBA-15

In this synthesis, the originator used was tetraethyl orthosilicate (TEOS) and the template used was P123.³⁵ The procedure is called sol-gel solution, and the solution is in acidic state.³⁶ First step, 10 mL ethanol was added to 62 g TEOS and stirred for 45 min at 25°C. Second, 10 mL ethanol was mixed with 18 mL HCl. This solution then was mixed with ethanol (20 mL) and 90 mL distilled water and stirred for 45 min. The mixed solution was then refluxed for 3 h at temperature of 60°C. Later, the surfactant solution was added drop wise into TEOS solution and kept on stirring awaiting the solution turned into gel. The obtained gel was dried at 100°C for an hour and calcined for 5 h before subjected for characterizations.

Quercetin Loading

SBA-15 particles were added into Q solution and incubated in a shaker at room temperature overnight. Q molecules could diffuse in solution into the pore channels. The Q-loaded SBA-15 was removed by centrifugation and rinsed with water to get rid of the redundant Q. Finally, the resulting particles were dried in vacuo at 60°C after being washed with water to yield Q-loaded SBA-15. The amount of Q-loaded into SBA-15 was determined by UV-VIS spectroscopy at 369 nm ($\lambda_{\max} = 369$ nm)³³

Loading Content

$$= \frac{\text{Initial weight of } Q - \text{Supernatant weight of } Q}{\text{Weight of particles}} \times 100\%$$

Characterizations

For TEM analysis, the dispersed ethanolic solution of material was sonicated for 5 min before placing onto the carbon-coated copper grid. FT-IR spectrum of the Q-SBA-15 prepared as KBr pellets was performed on a Perkin Elmer IR 783 spectrophotometer in the range of 4000–400 cm^{-1} .³⁷

Cell Culture and MTT Assay

The A549 cells were maintained in DMEM comprising 10% FBS with 1% antibiotic cocktail as per manufacturer's protocol. Propagation of the cells takes place in humidified incubator supplied with 5% CO_2 and maintained at 37°C. After

confluence (70–75%), cells were collected in PBS medium with EDTA (.52 mM) and trypsin (.25%) and plated at a suitable density to allow them to re-equilibrate before the examination.³⁸

To measure cell viability and proliferation forms, MTT (4,5-Dimethyl-thiazol-2-yl)-2,5-diphenyl tetrazolium bromide) assay was done.³⁹ In this assay, the cells were plated in 96 well plates (4×10^3 cells/well) and treated in presence and absence of different concentrations of Q and Q-SBA-15 for 24 h. After the incubation period of treatment, the cells were incubated with MTT solution for 4 h. The cells after treatment were incubated with MTT solution for 4 h. The yellow tetrazolium salt (MTT) decreases in metabolically active cells to form insoluble purple formazan crystals, which were solubilized by the addition of acidic isopropanol. The color change was determined spectrophotometrically at 595 nm *via* an ELISA reader. The same protocol has been followed for HEK 293. Each assay was repeated three times and in triplicate for each type of sample, and the cytotoxicity was evaluated using absorbance values as follows⁴⁰

$$\text{Cell viability} = \frac{\text{OD of Control} - \text{OD of treated}}{\text{OD of Control}} \times 100$$

Quantification of Apoptosis/Necrosis

During this process, properly washed control and treated A549 cells were stained with propidium iodide (PI) and Annexin V-FITC in agreement with the seller's guidelines (Calbiochem, Merck Millipore, Burlington, Massachusetts, United States).⁴¹ A flow cytometer (BD LSRFortessa, San Jose, CA, United States) was used to detect the percentages of early and/or late live, apoptotic, and necrotic cells. The observed data were investigated through the FlowJo software (version 10.0).

Immunofluorescence

Separately, control/treated A549 cells were washed twice for 10 min in PBS (.01 M) and incubated for 1 h in blocking solution having normal bovine serum (2%) and Triton X-100 (.3%).⁴² After this, the cells were incubated overnight at 4°C with the corresponding primary antibody (p-AKT, p-PI3K and *cytochrome c*), followed by washing and incubation with one-to-one fluorophore-conjugated secondary antibodies (antimouse/rabbit FITC and PE) for 2 h. Each slide was counterstained with nuclear dye (DAPI) for 10 min and mounted with the ProLong antifade reagent, which was identified by a confocal microscope. The dilution of primary and secondary was 1:500 and 1:100, respectively. Olympus FV10i microscope was used for the experiment. The data was analyzed by FluoView software.

Measurement of Caspase-9 Activity

Commercially available caspase-9 colorimetric assay kit (BioVision Research Products, Mountain View, CA) was

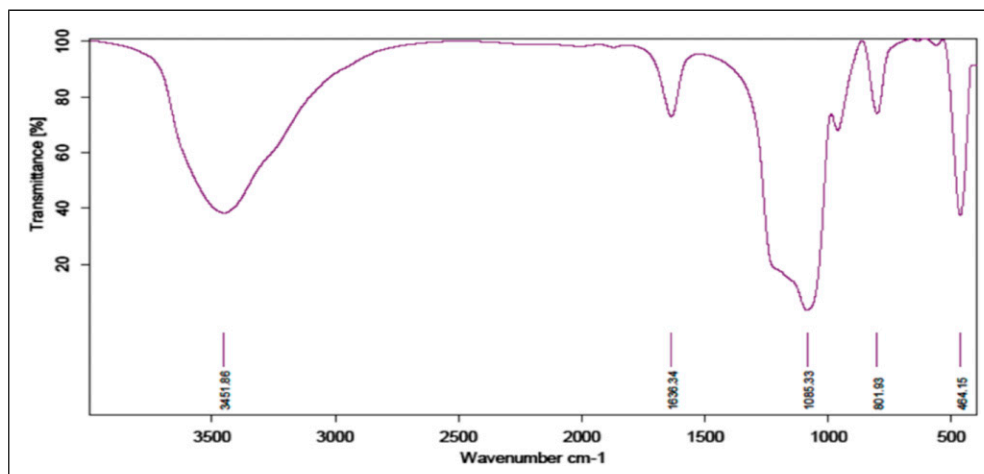


Figure 2. FTIR spectrum of synthesized Q-SBA-15 in the range of 4000–4400 cm^{-1} .

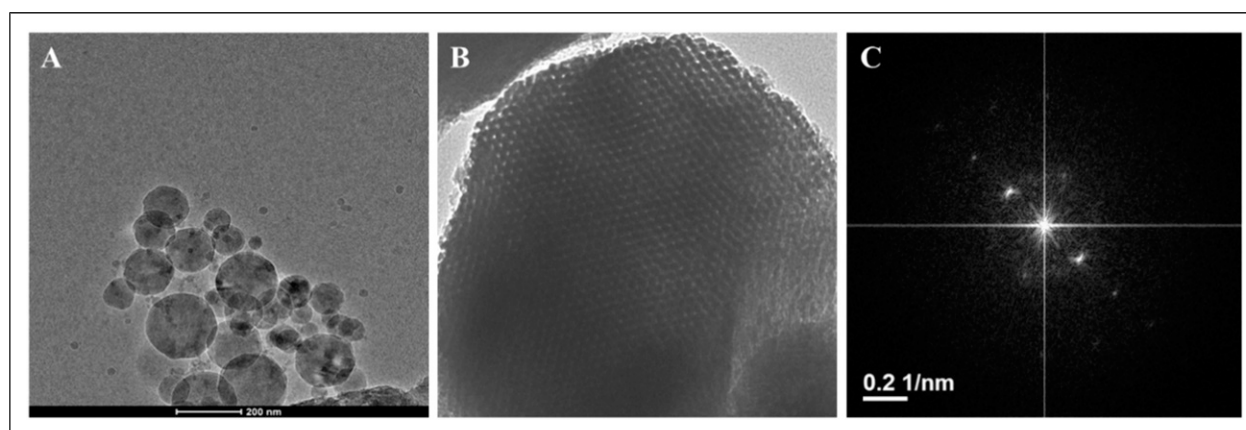


Figure 3. TEM images of synthesized SBA-15 (A) under 200 nm scale bar (B) under 10 nm scale bar (C). SAED pattern of SBA-15.

applied to determine the caspase-9 activities as per the manufacturer's protocols. Absorbance was recorded at 405 nm by an ELISA reader.⁴³

In Vitro Quercetin Release

The *in vitro* drug release experiments were conducted at different pHs 5.5 and 7.4 with 10 $\mu\text{g}/\text{mL}$ of Q-SBA-15 loaded into a dialysis bag; .01 mg of EDTFP-1 was dispersed in a known amount (1 mL) of PBS of 7.4 and 5.5 solutions, transferred to dialysis bag, and kept at 37°C. The resulting suspension was immersed into 10 mL of PBS and pH 5.5 solutions and incubated at 130 r/min for a definite time period (9 h). Five hundred microliter aliquots were drawn from the above dispersions after 30 min intervals; this was replaced by equal volume of the fresh PBS solution and pH 5.5 buffer for retaining the release medium same. Release of Q was studied through the UV spectrophotometric analysis at 370 nm.

Statistical Analysis

All values were presented as standard error mean ($\pm\text{SEM}$). Statistical meaning and differences among the set condition was evaluated through one-way analysis of variance (ANOVA) test followed by OriginPro 8.0 software. The critical significance level was set at $P < .05$.

Result and Discussion

Characterizations

The FT-IR spectrum of calcined Q-SBA-15 sample was recorded on Perkin Elmer IR 783 spectrophotometer (Figure 2). Q comprises of two benzene rings linked by pyran or pyrone. The spectrum displayed asymmetric and symmetric stretching vibrations bands at 1085 and 801 cm^{-1} , respectively, which belong to the Si–O–Si mesoporous silica in Q-SBA-15-conjugated framework. A weak band around 965 cm^{-1} represents Si–OH stretching. The band at 1636 cm^{-1} was credited to the

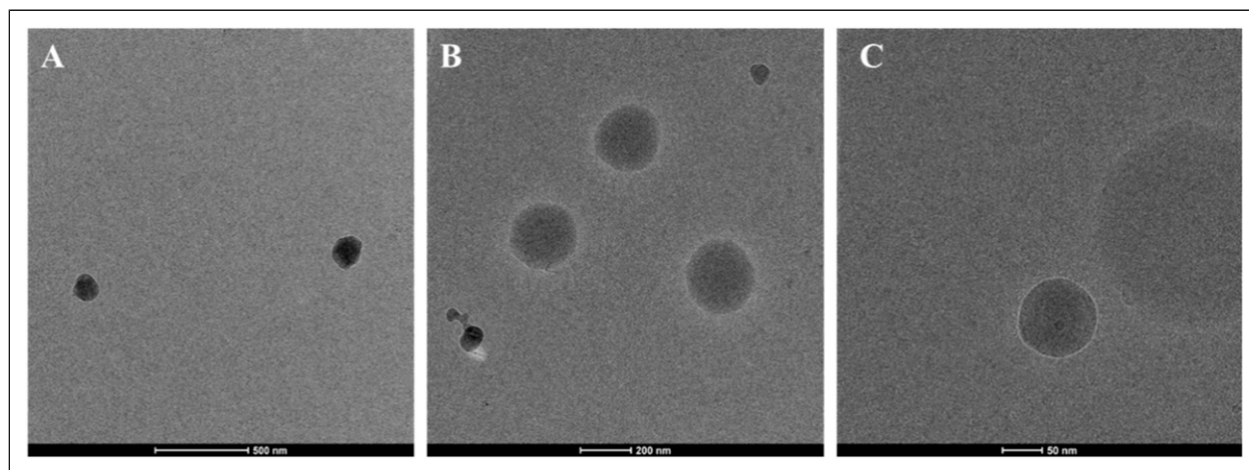


Figure 4. TEM images of synthesized Q-SBA-15 (A) under 500 nm scale bar (B) under 200 nm scale bar (C) under 50 nm scale bar.

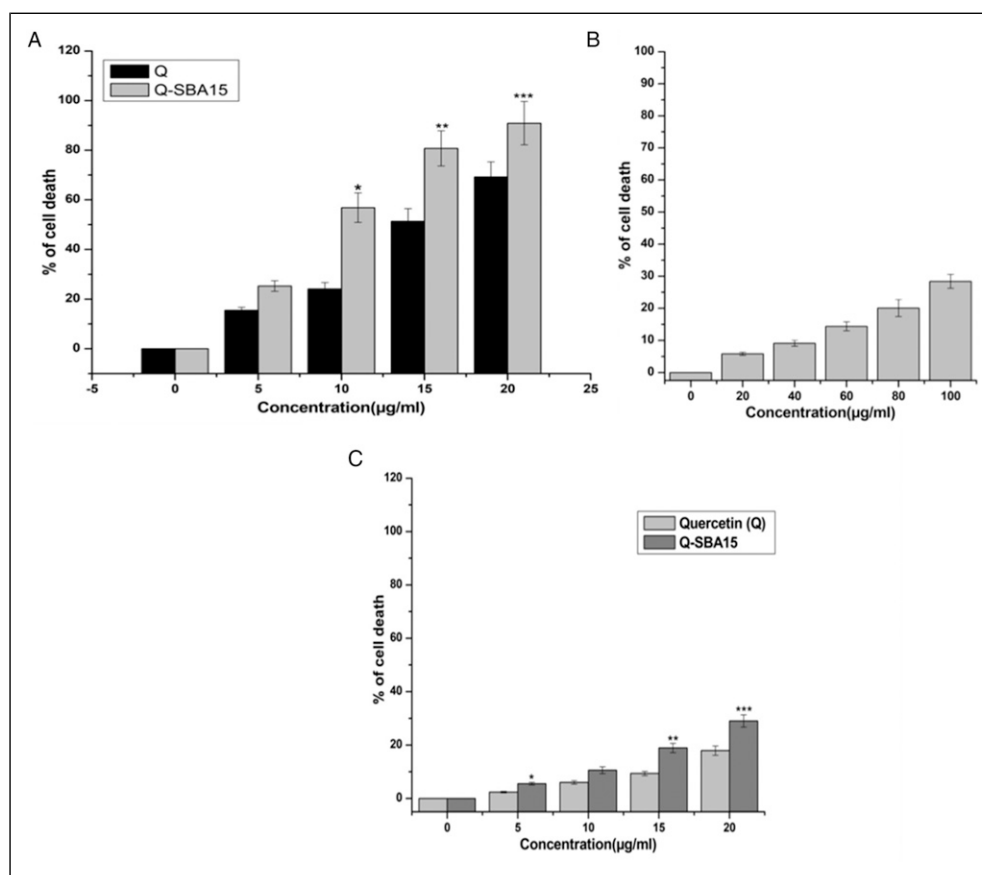


Figure 5. (A) MTT assay of Quercetin, Q-SBA-15, (B) only SBA-15 on A549 and (C) Q and Q-SBA-15 on HEK 293 cell line after 24 h of treatment; Each value represents the mean \pm SE of three experiments, $n = 3$, (* $P < .05$, ** $P < .01$, *** $P < .001$) compared with the control.

carboxyl group ($-C=O$) stretching vibration of Q and a broad envelop near 3451 cm^{-1} ascribed to the characteristic $-OH$ stretching vibration due to presence of phenolic group of Q.

High-resolution transmission electron microscopy (HRTEM) images and SAED pattern of SBA-15 nanoparticles are shown in Figure 3. It is evident from the Figure 3(A) that

hexagonally order pore channels of SBA-15 material were observed under 200 nm scale bar. The pores are observed in Figure 3(B), and the SAED pattern confirmed the mesoporous structure of SBA-15 (Figure 3(C)). After Q loading, the structure remains same (Figure 4) which revealed that there is no alteration in the SBA-15 after loading of Q.

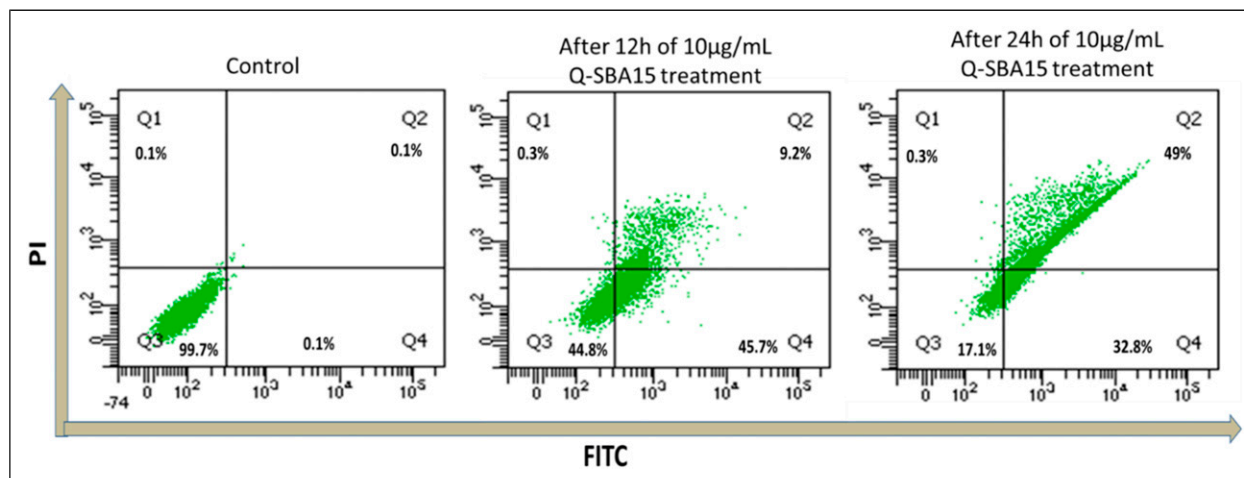


Figure 6. Annexin V-FITC/PI data after 12 and 24 h of 10 µg/mL Q-SBA-15 treatment against A549, where Q3, Q4, Q2, and Q1 indicate viable cell, early apoptosis, late apoptosis, and necrosis, respectively. Q-SBA-15 Dephosphorylated AKT/PI3K/mTOR pathway in A549 cells.

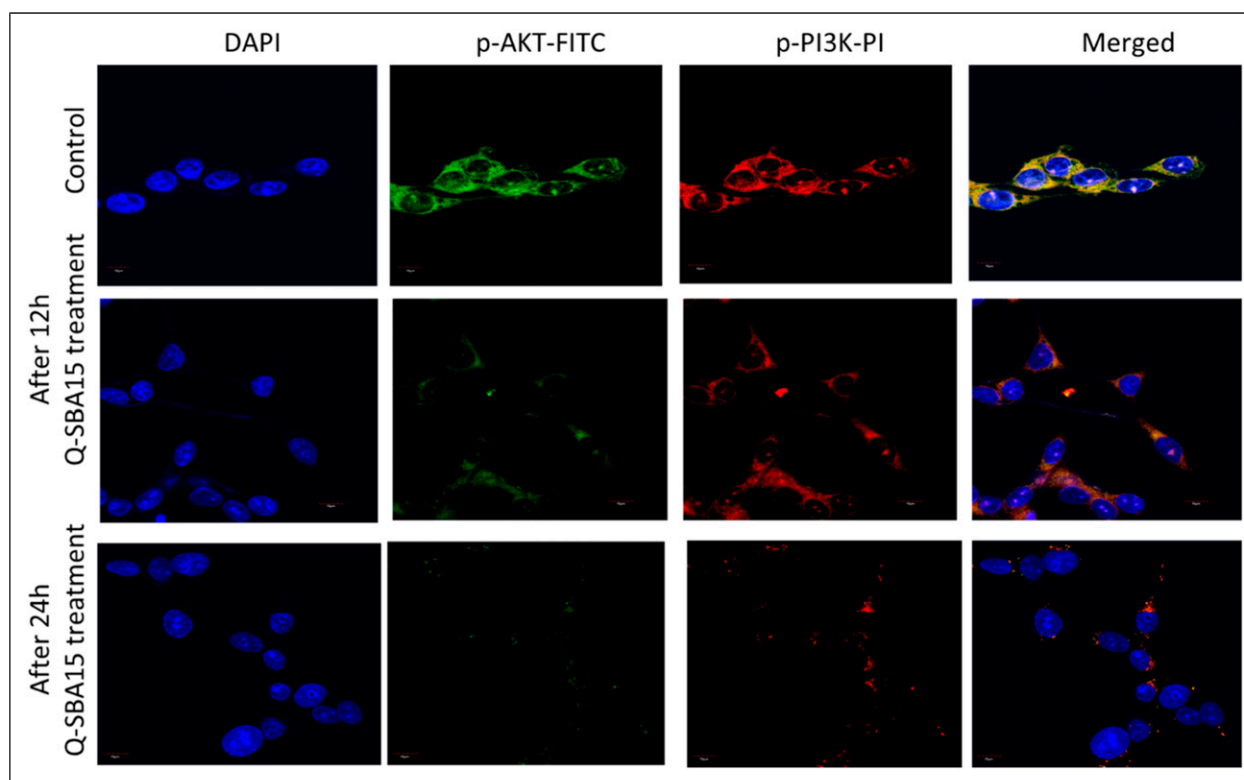


Figure 7. Expression of p-AKT and p-PI3K after 12 and 24 h of 10 µg/mL Q-SBA-15 treatment against A549, DAPI used as nuclear stainer.

MTT Assay

The MTT assay was carried out to evaluate the cytotoxicity of the Q and loaded with SBA-15 (Q-SBA-15) at the varying concentrations (0–20 µg/mL) against A549. The treatment of Q and Q-SBA-15 was for 24 h. In the event of A549 cell line, the colorimetric data (Figure 5) showed that after 15 µg/mL of Q-SBA-15 treatment, almost all the cells were dead, whereas in

case of Q, the dose was 25 µg/mL. While in case of Q alone, the data implicated that 30, 50, and 70% cells were dead at 12.35, 20.09, and 26.82 µg/mL, respectively, after 24 h of treatment. The cytotoxicity of only SBA-15 was also evaluated, which displays insignificant effect up to 40 µg/mL of concentration. However, Q-SBA-15 conjugated system exhibited IC₃₀, 50, and 70 doses at 6.29, 9.57, and 16.5 µg/mL, respectively. From this data, we have established that Q-SBA-15 is more potent

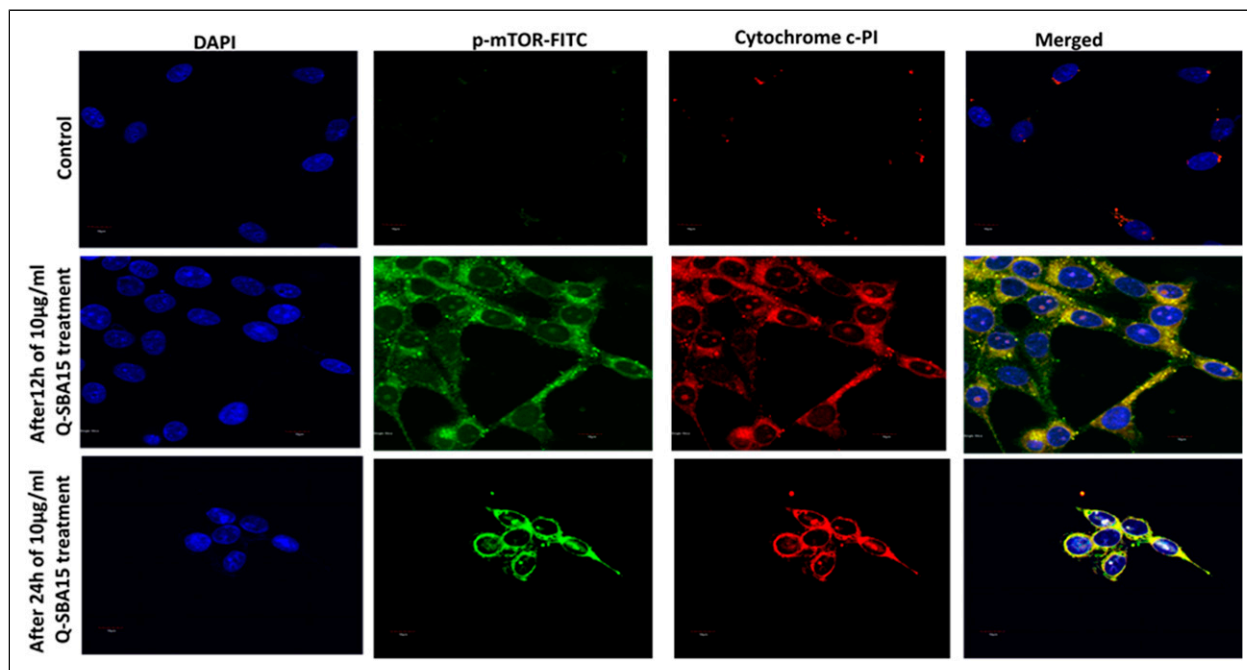


Figure 8. Expression of p-mTOR and *cytochrome c* after 12 and 24 h of 10 µg/mL Q-SBA-15 treatment against A549, DAPI used as nuclear stainer.

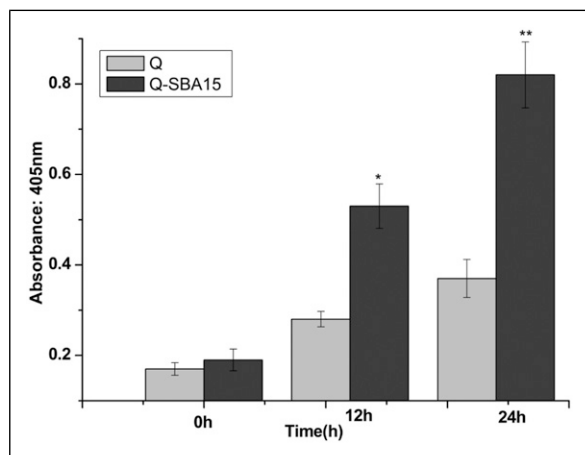


Figure 9. Expression of caspase-9 after 12 and 24 h of 10 and 20 µg/mL Q-SBA-15 and Q, respectively. Each value represents the mean \pm SE of three experiments, $n = 3$, (* $P < .05$, ** $P < .01$) compared with control.

(85% of cells death) than only Q (65% of cells death) at the same concentration 20 µg/mL. We have also checked the cytotoxicity of Q-SBA-15 on HEK-293 cell line; up to 20 µg/mL, there was no such kind of toxicity. So 9.57 µg/mL dose was selected for further biological experiments.

Q-SBA-15 Induced Apoptosis in A549 Cells

It is established that phosphatidylserine (PS), a phospholipid component, translocated in the cell membrane and

externalized during apoptosis process. Annexin-V is a specific PS-binding protein that can be used to distinguish the apoptotic cells when conjugated with an exact fluorophore. Interestingly, as shown in Figure 6, the percentage of early and late apoptotic population increased progressively after 10 µg/mL of Q-SBA-15 treatment in time-dependent manner (12 and 24 h). With 12 h of Q-SBA-15 treatment, the viable cells were reduced to 44.8% following the enhancement of early/late apoptotic and necrotic population of 45.7, 9.2, and .3%, respectively. After 24 h of treatment, the viable cells decreased to 17.1% following the early/late apoptotic and necrotic population of 32.8%, 49, and .3%. This data confirmed that Q-SBA-15 induced cell death is due to apoptosis.

Regulating PI3K/AKT/mTOR pathway in cancer cells acts a key aspect to make cancer cell viable for cell death during apoptosis. After treatment with 10 µg/mL of Q-SBA-15, the expression of p-AKT, p-PI3K, and p-mTOR was checked by confocal microscopy. As shown in Figure 7, it has been clearly exposed that the expression of p-AKT and p-PI3K has been decreased over the control one, after treatment of 10 µg/mL of Q-SBA-15 in time-dependent manner, where DAPI is used as nuclear stainer. As p-AKT down-regulates after treatment of Q-SBA-15, the expression of p-mTOR and *cytochrome c* has been analyzed by confocal microscopy (Figure 8). The data has shown that the enhancement in the expression of p-mTOR and *cytochrome c* has been observed in a time-dependent manner. Hence, from the microscopic images, it has been indicated that the Q-SBA-15-mediated apoptosis occurs *via* PI3K/AKT/mTOR signaling pathway.

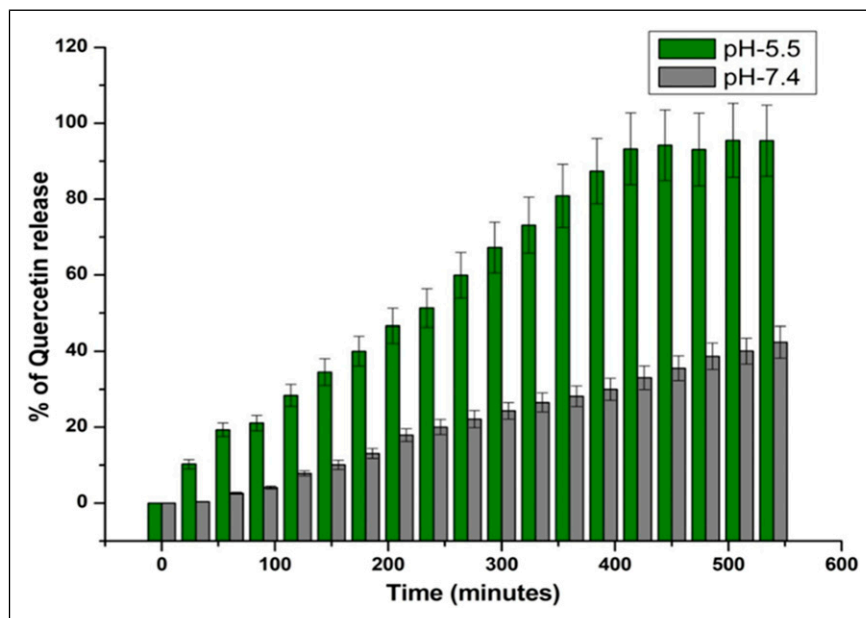


Figure 10. *In vitro* time-dependent pharmacokinetics of Q release from Q-SBA-15 at pH of 5.5 and 7.4.

Expression of Caspase-9 Activity

In order to corroborate the Q-SBA-15 induced cell death *via* PI3K/AKT/mTOR signaling pathway, the caspase-9 assay has been performed with different time interval. The expression of *cytochrome c* has been increased after treatment of Q-SBA-15 with respect to time. The final apoptotic fate was determined by the activity of caspase-9 (Figure 9), which was simultaneously enhanced with the treatment of Q-SBA-15 in a time-dependent manner. Thus, we concluded that Q-SBA-15-mediated apoptosis might be regulated through the PI3K/AKT/mTOR signaling pathway.

In Vitro Quercetin Release

In vitro Q release of Q-SBA-15 was evaluated at pH 5.5 and 7.4 as shown in Figure 10. The data shows that at acidic pH, the release of Q was found to be much higher at pH 7.4 as we know the pH of cancer cell is around 5.5. Therefore, we can tell that the apoptosis rate of Q-SBA-15 is much higher than only Q because of the pH-dependent delivery of Q-SBA-15.

Conclusion

In this study, Q-loaded Q-SBA-15 NPs were obtained by a multistep process. This study confirmed that the efficacy of Q-SBA-15 is much higher than only Q. In addition, the obtained data of apoptotic pathway suggested that the Q-SBA-15-mediated cell death is caspase-mediated apoptosis *via* PI3K/AKT/mTOR signaling pathway. Thus, Q-SBA-15 NPs have a huge prospective to be employed as an anticancer agent to overcome the epidemiology of lung cancer in future.

However, further investigations are needed to be conducted on different *in vitro* and *in vivo* experimental models.

Acknowledgments

The authors extend their appreciation to the Deanship of Scientific Research at King Saud University for funding this work through research group No. (RG-1441-536).

Author Contributions

NA and HA synthesized mesoporous SBA-15 and performed cell culture and treatments. SA and HA evaluated the cell viability and cell death. AA and SA measured the activity of caspases and data analysis. SA was involved in the conception and design of the study, data interpretation and critically revised the article. All authors read and approved the final article.

Declaration of Conflicting Interests

The authors declared no potential conflicts of interest with respect to the research, authorship, and/or publication of this article.

Funding

The authors disclosed receipt of the following financial support for the research, authorship, and/or publication of this article: The authors extend their appreciation to the Deanship of Scientific Research at King Saud University for funding this work through research group No (RG-1441-536).

ORCID iDs

Saad Alkahtani  <https://orcid.org/0000-0001-7381-5110>
Saud Alarifi  <https://orcid.org/0000-0002-3613-5228>

Data Availability

The data generated or analyzed in this article are online publicly available without request.

References

- Travis W, Rekhtman N. Pathological diagnosis and classification of lung cancer in small biopsies and cytology: Strategic management of tissue for molecular testing. *Semin Respir Crit Care Med*. 2011;32(1):022-031. doi:10.1055/s-0031-1272866
- Fu XL, Zhu XZ, Shi DR, et al. Study of prognostic predictors for non-small cell lung cancer. *Lung Cancer*. 1999;23(2):143-152. doi:10.1016/S0169-5002(99)00009-4
- Parashar B, Arora S, Wernicke A. Radiation therapy for early stage lung cancer. *Semin Intervent Radiol*. 2013;30(2):185-190. doi:10.1055/s-0033-1342960
- Xingyu Z, Peijie M, Dan P, et al. Quercetin suppresses lung cancer growth by targeting aurora b kinase. *Cancer Med*. 2016; 5(11):3156-3165. doi:10.1002/cam4.891
- Hariri G, Han Z, Hallahan D. Radiation-guided drug delivery of nanoparticle albumin-bound paclitaxel to lung cancer. *Int J Radiat Oncol*. 2008;72(1):S705-S706. doi:10.1016/j.ijrobp.2008.06.531
- Shi S, Vissapragada R, Abi Jaoude J, et al. Evolving role of biomaterials in diagnostic and therapeutic radiation oncology. *Bioact Mater*. 2020;5(2):233-240. doi:10.1016/j.bioactmat.2020.01.011.
- Li Y, Wang Z, Jin J, et al. Quercetin pretreatment enhances the radiosensitivity of colon cancer cells by targeting notch-1 pathway. *Biochem Biophys Res Commun*. 2020;523(4):947-953. doi:10.1016/j.bbrc.2020.01.048
- Baskar R, Lee KA, Yeo R, Yeoh KW. Cancer and radiation therapy: Current advances and future directions. *Int J Med Sci*. 2012;9(3):193-199. doi:10.7150/ijms.3635
- Fan W, Bu W, Zhang Z, et al. X-ray radiation-controlled no-release for on-demand depth-independent hypoxic radiosensitization. *Angew Chem Int Ed*. 2015;54(47):14026-14030. doi:10.1002/anie.201504536
- Song G, Chen Y, Liang C, et al. Catalase-loaded taox nanoshells as bio-nanoreactors combining high-z element and enzyme delivery for enhancing radiotherapy. *Adv Mater*. 2016;28(33): 7143-7148. doi:10.1002/adma.201602111
- Huang C, Chen T, Zhu D, Huang Q. Enhanced tumor targeting and radiotherapy by quercetin loaded biomimetic nanoparticles. *Front Chem*. 2020;8:8. doi:10.3389/fchem.2020.00225
- Bigdeli B, Goliaei B, Masoudi-Khoram N, et al. Enterolactone: A novel radiosensitizer for human breast cancer cell lines through impaired dna repair and increased apoptosis. *Toxicol Appl Pharmacol*. 2016;313:180-194. doi:10.1016/j.taap.2016.10.021
- Wang Q, Chen Y, Lu H, et al. Quercetin radiosensitizes non-small cell lung cancer cells through the regulation of mir-16-5p/wee1 axis. *IUBMB Life*. 2020;72(5):1012-1022. doi:10.1002/iub.2242
- Kang J, Kim E, Kim W, et al. Rhamnetin and cirsiolol induce radiosensitization and inhibition of epithelial-mesenchymal transition (emt) by mir-34a-mediated suppression of notch-1 expression in non-small cell lung cancer cell lines. *J Biol Chem*. 2013;288(38):27343-27357. doi:10.1074/jbc.M113.490482
- Wang Y, Yu H, Wang S, et al. Targeted delivery of quercetin by nanoparticles based on chitosan sensitizing paclitaxel-resistant lung cancer cells to paclitaxel. *Mater Sci Eng C*. 2021;119: 111442. doi:10.1016/j.msec.2020.111442
- Lin C, Yu Y, Zhao H, Yang A, Yan H, Cui Y. Combination of quercetin with radiotherapy enhances tumor radiosensitivity *in vitro* and *in vivo*. *Radiother Oncol*. 2012;104(3):395-400. doi: 10.1016/j.radonc.2011.10.023
- Kale A, Ö P, Baş Y, et al. Neuroprotective effects of quercetin on radiation-induced brain injury in rats. *J Radiat Res*. 2018;59(4): 404-410. doi:10.1093/jrr/rry032
- Pérez-Cano FJ, Castell M. Flavonoids, inflammation and immune system. *Nutrients*. 2016;8(10):659. doi:10.3390/nu8100659
- Chang JH, Lai SL, Chen WS, et al. Quercetin suppresses the metastatic ability of lung cancer through inhibiting snail-dependent akt activation and snail-independent adam9 expression pathways. *Biochim Biophys Acta Mol Cell Res*. 2017;1864(10):1746-1758. doi:10.1016/j.bbamcr.2017.06.017
- Mukherjee A, Mishra S, Kotla NK, et al. Semisynthetic quercetin derivatives with potent antitumor activity in colon carcinoma. *ACS Omega*. 2019;4(4):7285-7298. doi:10.1021/acsomega.9b00143
- Zheng SY. Anticancer effect and apoptosis induction by quercetin in the human lung cancer cell line A-549. *Mol Med Rep*. 2011;5(3):822-826. doi:10.3892/mmr.2011.726
- Ma T, Liu Y, Wu Q, et al. Quercetin-modified metal-organic frameworks for dual sensitization of radiotherapy in tumor tissues by inhibiting the carbonic anhydrase IX. *ACS Nano*. 2019;13(4):4209-4219. doi:10.1021/acsnano.8b09221
- Gibellini L, Pinti M, Nasi M, et al. Quercetin and cancer chemoprevention. Evidence-Based Complement. *Altern Med*. 2011;2011:591356. doi:10.1093/ecam/nej053
- Gong C, Yang Z, Zhang L, Wang Y, Gong W, Liu Y. Quercetin suppresses dna double-strand break repair and enhances the radiosensitivity of human ovarian cancer cells *via* p53-dependent endoplasmic reticulum stress pathway. *OncoTargets Ther*. 2017;11:17-27. doi:10.2147/OTT.S147316
- Han EJ, Im CN, Park SH, Moon EY, Hong SH. Combined treatment with peroxisome proliferator-activated receptor (ppar) gamma ligands and gamma radiation induces apoptosis by ppar-independent up-regulation of reactive oxygen species-induced deoxyribonucleic acid damage signals in non-small cell lung. *Int J Radiat Oncol*. 2013;85(5):e239-e248. doi:10.1016/j.ijrobp.2012.11.040
- Liu H, Xue JX, Li X, Ao R, Lu Y. Quercetin liposomes protect against radiation-induced pulmonary injury in a murine model. *Oncol Lett*. 2013;6(2):453-459. doi:10.3892/ol.2013.1365
- Madamanchi NR, Hakim ZS, Runge MS. Oxidative stress in atherogenesis and arterial thrombosis: The disconnect between cellular studies and clinical outcomes. *J Thromb Haemost*. 2005; 3(2):254-267. doi:10.1111/j.1538-7836.2004.01085.x

28. Rauf A, Imran M, Khan IA, et al. Anticancer potential of quercetin: A comprehensive review. *Phyther Res.* 2018;32(11): 2109-2130. doi:10.1002/ptr.6155
29. Gao X, Huang N, Shi H, et al. Enhancing the anti-colon cancer activity of quercetin by self-assembled micelles. *Int J Nanomed.* 2015;10:2051-2063. doi:10.2147/IJN.S75550
30. Vafadar A, Shabaninejad Z, Movahedpour A, et al. Quercetin and cancer: New insights into its therapeutic effects on ovarian cancer cells. *Cell Biosci.* 2020;10(1):32. doi:10.1186/s13578-020-00397-0
31. Verma P, Kuwahara Y, Mori K, Raja R, Yamashita H. Functionalized mesoporous sba-15 silica: recent trends and catalytic applications. *Nanoscale.* 2020;12(21):11333-11363. doi:10.1039/D0NR00732C
32. Liu B, Jiang T, Zheng H, et al. Nanoengineering of aggregation-free and thermally-stable gold nanoparticles in mesoporous frameworks. *Nanoscale.* 2017;9(19):6380-6390. doi:10.1039/C7NR01988B
33. Mishra S, Manna K, Kayal U, et al. Folic acid-conjugated magnetic mesoporous silica nanoparticles loaded with quercetin: A theranostic approach for cancer management. *RSC Adv.* 2020; 10(39):23148-23164. doi:10.1039/D0RA00664E
34. Vavsari VF, Ziarani GM, Badii A. The role of SBA-15 in drug delivery. *RSC Adv.* 2015;5(111):91686-91707. doi:10.1039/C5RA17780D
35. Björk EM. Synthesizing and characterizing mesoporous silica SBA-15: A hands-on laboratory experiment for undergraduates using various instrumental techniques. *J Chem Educ.* 2017; 94(1):91-94. doi:10.1021/acs.jchemed.5b01033
36. Pirez C, Morin JC, Manayil JC, Lee AF, Wilson K. Sol-gel synthesis of SBA-15: impact of HCl on surface chemistry. *Microporous Mesoporous Mater.* 2018;271:196-202. doi:10.1016/j.micromeso.2018.05.043
37. Park SY, Pendleton P. Mesoporous silica SBA-15 for natural antimicrobial delivery. *Powder Technol.* 2012;223:77-82. doi: 10.1016/j.powtec.2011.08.020
38. Stern R. Association between cancer and “acid mucopolysaccharides”: an old concept comes of age, finally. *Semin Cancer Biol.* 2009;18(4):238-243. doi:10.1016/B978-012374178-3.10001-8
39. Ali A, Mishra S, Kamaal S, et al. Evaluation of cathecolase mimicking activity and apoptosis in human colorectal carcinoma cell line by activating mitochondrial pathway of copper(II) complex coupled with 2-(quinolin-8-yloxy)(methyl)benzotrile and 8-hydroxyquinoline. *Bioorg Chem.* 2021;106:104479. doi: 10.1016/j.bioorg.2020.104479
40. Mohammed MO, Alkubaisi HMM, Haj NQ. A new prodrug and bioactivity evaluation of methotrexate based on chitosan. *Heliyon.* 2020;6(6):e04223. doi:10.1016/j.heliyon.2020.e04223
41. Sato K, Nishii T, Sato A, Tatsunami R. Autophagy activation is required for homocysteine-induced apoptosis in bovine aorta endothelial cells. *Heliyon.* 2020;6(1):e03315. doi:10.1016/j.heliyon.2020.e03315
42. Sau A, Sanyal S, Bera K, et al. DNA damage and apoptosis induction in cancer cells by chemically engineered thiolated riboflavin gold nanoassembly. *ACS Appl Mater Inter.* 2018; 10(5):4582-4589. doi:10.1021/acsami.7b18837
43. Bhanja P, Mishra S, Manna K, Mallick A, Saha KD, Bhaumik A. Covalent organic framework material bearing phloroglucinol building units as a potent anticancer agent. *ACS Appl Mater Inter.* 2017;9(37):31411-31423. doi:10.1021/acsami.7b07343

Appendix A

DAPI	6-diamidino-2-phenylindole
DMEM	Dulbecco's Modified Eagle Medium
EDTA	ethylenediaminetetraacetic acid
FBS	fetal bovine serum
FITC	fluorescein isothiocyanate
FTIR	Fourier-transform infrared spectroscopy
IR	ionizing radiation
P123	poly(ethylene glycol)-block-poly(propylene glycol)-block-poly(ethylene glycol)
PBS	phosphate-buffered saline
PE	phycoerythrin
PI	propidium iodide
PSN	penicillin-streptomycin-neomycin
Q	quercetin
ROS	reactive oxygen species
RT	radiation therapy
TEM	transmission electron microscopy
TEOS	tetraethyl orthosilicate